1-1-2015

Technical Note: Phantom study to evaluate the dose and image quality effects of a computed tomography Organ-based Tube Current Modulation Technique

Diksha Gandhi
Marquette University

Dominic J. Crotty
GE Healthcare

Grant M. Stevens
GE Healthcare

Taly Gilat Schmidt
Marquette University, tal.gilat-schmidt@marquette.edu

Accepted version. *Medical Physics*, Vol. 42 (2015): 6572-6578. DOI.

Technical Note: Phantom Study to Evaluate the Dose and Image Quality Effects of a Computed Tomography Organ-Based Tube Current Modulation Technique

Diksha Gandhi
Department of Biomedical Engineering, Marquette University
Milwaukee, WI
Dominic J. Crotty
GE Healthcare
Waukesha, WI
Grant M. Stevens
GE Healthcare
Waukesha, WI
Taly Gilat Schmidt
Department of Biomedical Engineering, Marquette University
Milwaukee, WI

Medical Physics, Vol. 42 (2015): pg. 6572-6578. DOI.

Abstract

Purpose: This technical note quantifies the dose and image quality performance of a clinically available organ-dose-based tube current modulation (ODM) technique, using experimental and simulation phantom studies. The investigated ODM implementation reduces the tube current for the anterior source positions, without increasing current for posterior positions, although such an approach was also evaluated for comparison.
Methods: Axial CT scans at 120 kV were performed on head and chest phantoms on an ODM-equipped scanner (Optima CT660, GE Healthcare, Chalfont St. Giles, England). Dosimeters quantified dose to breast, lung, heart, spine, eye lens, and brain regions for ODM and 3D-modulation (SmartmA) settings. Monte Carlo simulations, validated with experimental data, were performed on 28 voxelized head phantoms and 10 chest phantoms to quantify organ dose and noise standard deviation. The dose and noise effects of increasing the posterior tube current were also investigated.
Results: ODM reduced the dose for all experimental dosimeters with respect to SmartmA, with average dose reductions across dosimeters of 31% (breast), 21% (lung), 24% (heart), 6% (spine), 19% (eye lens), and 11% (brain), with similar results for the simulation validation study. In the phantom library study, the average dose reduction across all phantoms was 34% (breast), 20% (lung), 8% (spine), 20% (eye lens), and 8% (brain). ODM increased the noise standard deviation in reconstructed images by 6%–20%, with generally greater noise increases in anterior regions. Increasing the posterior tube current provided similar dose reduction as ODM for breast and eye lens, increased dose to the spine, with noise effects ranging from 2% noise reduction to 16% noise increase. At noise equal to SmartmA, ODM increased the estimated effective dose by 4% and 8% for chest and head scans, respectively. Increasing the posterior tube current further increased the effective dose by 15% (chest) and 18% (head) relative to SmartmA.
Conclusions: ODM reduced dose in all experimental and simulation studies over a range of phantoms, while increasing noise. The results suggest a net dose/noise benefit for breast and eye lens for all studied phantoms, negligible lung dose effects for two phantoms, increased lung dose and/or noise for eight phantoms, and increased dose and/or noise for brain and spine for all studied phantoms compared to the reference protocol.

Key Topics: Medical image noise, Lungs, Brain, Tissues, Dosimetry

1. Introduction

Increasing concern about the risks of radiation from routine CT scans has prompted research into methods for reducing radiation dose, with emphasis in reducing dose to radiosensitive tissues such as the eye lens and breast. Previous studies investigated organ-based tube current modulation (TCM) techniques that reduce tube current for the anterior views and increase tube current for posterior views.[1–7]

Medical Physics, Vol. 42 (2015): pg. 6572-6578. DOI.

Increased tube current for the posterior views increased the absorbed dose in spine, lung, and other tissues.[1–7,24] Bismuth shields were also proposed to reduce dose to anterior organs, although with increased image degradations.[2,8,9] Studies have shown that if the noise increase due to shields is acceptable, equal or lower dose can be obtained by global tube current reduction.[1,2]

This study evaluated a commercially available organ-dose-based tube current modulation (ODM) implementation that performs targeted tube current reduction by decreasing the tube current for a range of anterior views without increasing the tube current for the posterior views. Different ODM protocols are available for chest and head scans, with the goal of reducing dose to the breast (for female patients) and eye lens, respectively. This study quantified the radiation dose and noise standard deviation effects of this specific ODM implementation compared to the reference protocol on the same scanner. The dose and noise effects of increasing the posterior tube current to maintain the same mAs as the reference scan were also investigated.

2. Methods and Materials

This study investigated the dose and image quality performance of a specific organ-based tube current modulation technique (ODM, GE Healthcare, Chalfont St. Giles, UK). ODM was compared to the reference 3D modulation technique (SmartmA, GE Healthcare, Chalfont St. Giles, UK) that varies the current in both the slice and angular directions based on estimates of patient attenuation obtained from scout images. As can be seen in Fig. 1, SmartmA varies tube current in the angular direction, with the minimum and maximum values depending on factors such as the patient attenuation at that scan-location and the prescribed noise index. ODM is a modification to SmartmA that further reduces tube current for the anterior views while maintaining the SmartmA settings for the remaining views. Routine head and chest scans experience tube current reduction of approximately 30% and 40% across 100◦ and 160◦ of anterior views, respectively. For the phantom that generated Fig. 1, ODM used 80% of the photons of the SmartmA scan.

Medical Physics, Vol. 42 (2015): pg. 6572-6578. DOI.

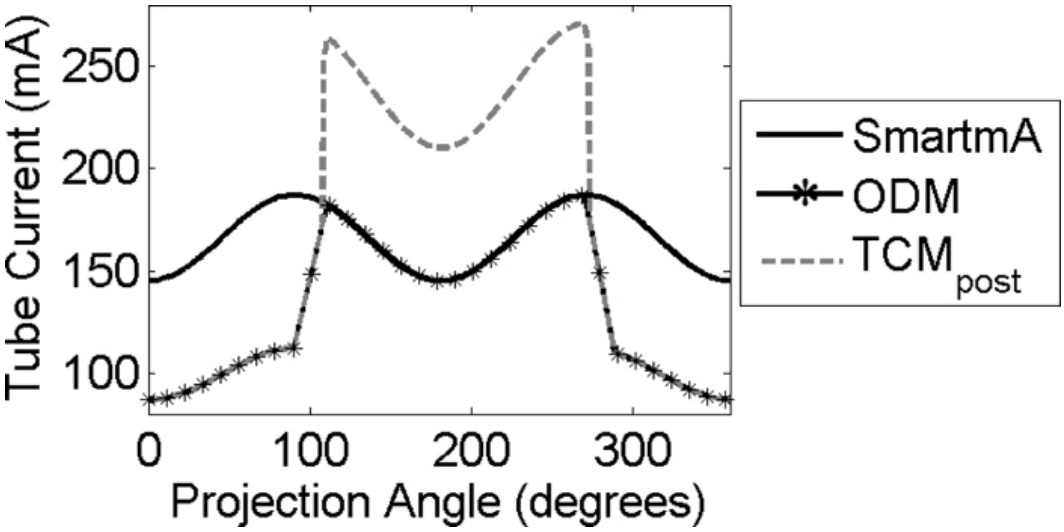

FIG. 1. Tube current at each projection angle for one scan rotation of a chest phantom. An angle of zero degrees refers to the AP view.

For the phantom library study (Sec. 2.C), an additional tube current modulation technique was simulated to investigate the dose and noise effects of increasing the posterior tube current to compensate for the decreased anterior tube current. The simulated tube current modulation method (TCM_{post}) was calculated to have the same anterior tube current as ODM, with the tube current in the remaining views increased to match the total mAs of SmartmA for each rotation, as illustrated in Fig. 1. The specific TCM_{post} modulation scheme simulated in this study is not commercially available.

2.A. Experimental methods

Axial CT scans at 120 kV were performed on anthropomorphic head and chest phantoms (Rando Alderson Research Laboratories, Stanford, CA) on an ODM-equipped scanner (Optima CT660, GE Healthcare, Chalfont St. Giles, England). The effects of ODM were studied using axial exams to avoid the confounding effects of helical start angle, which can significantly affect some organ doses.[10–12] Thirteen MOSFET dosimeters (mobile MOSFET Dosimetry System, Best Medical, Ottawa, Canada) were placed at tissue locations in the breast, lung, heart, eye lens, and brain regions to quantify radiation dose. Because the spine region was inaccessible for dosimeter placement, a

Medical Physics, Vol. 42 (2015): pg. 6572-6578. DOI.

dosimeter was placed in the posterior region of the lung in the closest insert to the spine region to estimate dose changes in the posterior "spine" region.

For each phantom, five scans were performed with SmartmA and ODM, with all other scan parameters held constant. Head scans were performed using seven axial rotations, 0.5 cm slice thickness, and 14 cm total scan range. The noise index was held constant at 2.8, resulting in a $CTDI_{vol}$ of 43.27 mGy for SmartmA and 41.27 mGy for ODM. The chest phantom was scanned with six axial rotations, 0.25 cm slice thickness, and 24 cm total scan range. The noise index was set to 7.0 resulting in a $CTDI_{vol}$ of 21.2 mGy for SmartmA and 17.1 mGy for ODM. For each dosimeter, the relative change in dose with respect to SmartmA was calculated. To assess the effect of ODM on image noise, the standard deviation was calculated in three 15 × 15 pixel regions of interest (ROIs) in the brain and chest regions of all reconstructed images.

2.B. Simulation methods

The CT system was modeled in geant4 (Ref. 13) with a 120 kV spectrum[14] and with beam collimation and number of rotations as in the experiments. A beam-shaping bowtie filter was also modeled using the information provided in the literature.[15] The output of the Monte Carlo simulations was the absorbed energy in electron volt at each voxel location of the phantom for each view angle and gantry scan-location. The absorbed energy was summed across all voxels in a segmented tissue region. The total absorbed energy for each tissue type was used as a surrogate for absorbed dose when calculating the relative change in dose for ODM compared to SmartmA.

Polyenergetic ray-tracing simulations were also implemented to generate simulated projections at the same angular sampling as the experiment. The simulations modeled Poisson noise and did not include electronic noise. The ray-tracing simulation software also generated an AP scout for all voxelized phantoms. This scout was input to the proprietary tube current modulation algorithm to determine the tube current for each view angle and gantry scan-location for SmartmA and ODM.

Medical Physics, Vol. 42 (2015): pg. 6572-6578. DOI.

This study compared the relative dose and noise performance of SmartmA and ODM, which depends on the shape of the tube current profiles (Fig. 1), but not the absolute number of photons. For Monte Carlo dose simulations, the total number of simulated photons was empirically determined to provide deposited energy estimates with low standard deviation (<1%) between trials. For the ray-tracing simulations, the tube current profiles were multiplied by an empirically determined scaling factor of 7.4×10^5 photons/mA for each ray to achieve reconstructed noise standard deviation of approximately 7–20 HU. All data were reconstructed using the same in-house filtered backprojection algorithm.

The simulation workflow was validated by performing simulations on a voxelized version of the experimental anthropomorphic phantoms. To create the phantom, the volume of experimental axial head and chest images was segmented into four materials: air (<−200 HU), water (−200 to 5 HU), soft tissue (5–280 HU), and bone (>280 HU), with attenuation coefficient obtained from the NIST XCOM database.[16] Tube current profiles were generated from simulated AP scout images of these phantoms for SmartmA and ODM settings using proprietary software. The dosimeter locations in the experimental images were segmented in the voxelized phantoms. The absorbed dose to the dosimeter locations was estimated using the Monte Carlo simulation software. The percent change in dose for ODM with respect to SmartmA was compared for both experimental and simulated results. Relative noise with respect to SmartmA was then compared for both experimental and simulated reconstructed images.

2.C. Voxelized phantom library study

Voxelized phantoms were simulated from the extended cardiac-torso (XCAT) phantom library[17] to study the ODM dose and image quality effects for patients of varying sizes and anatomy. For the purpose of this study, the head phantoms were segmented into eight materials: air, water, brain, blood, cartilage, bone, muscle, and eye lens, while the chest phantoms were segmented into eleven materials: air, lung, soft tissue, muscle, adipose, glandular breast, blood, bone, water, spinal cord, and cartilage. The glandular breast tissue was segmented and modeled as 100% glandular tissue, with the remaining

Medical Physics, Vol. 42 (2015): pg. 6572-6578. DOI.

breast modeled as adipose tissue. The x-ray mass attenuation values for the segmented materials were obtained from NIST.[16] Blood in the chest phantom was modeled as a mixture of water and iodine with 0.28 mg/ml iodine concentration. This study used a total of 28 head (15 male and 13 female) and 10 chest (all female) phantoms from the XCAT library. The body mass index (BMI) of the voxelized phantoms ranged from 18.2 to 36.7 with an average BMI of 27.3. Monte Carlo and ray-tracing simulations were performed as described in Sec. 2.B. The Monte Carlo simulations estimated the percent change in dose for ODM and TCM_{post} compared to SmartmA in the brain and eye lens (head scans) and breast, lung, heart, and spine (chest scans). The noise standard deviation of SmartmA compared to ODM and TCM_{post} was calculated in ROIs in the heart, anterior lung, and posterior lung regions for the reconstructed chest images, and in anterior, center, and posterior brain regions for the head images.

The effect of patient size was investigated by calculating the effective diameter of each head and chest phantom.[18] To determine which organs exhibit a net benefit in dose and/or noise, a cost–benefit analysis was performed on the phantom library simulation results by plotting relative noise versus relative dose of ODM compared to SmartmA. To investigate the effects of increasing the posterior tube current to compensate for the photons removed in the anterior views, the same cost–benefit plot was generated for the TCM_{post} modulation method.

The overall dose effects of ODM and TCM_{post} were compared relative to SmartmA by estimating the effective dose of both techniques at noise standard deviation equal to SmartmA. For each phantom and scan type (head or chest), the dose to each tissue type, d, was calculated by dividing the deposited energy by the total mass of that tissue in the phantom. The metric of effective dose, $\widetilde{D}$eff, was estimated for both ODM and TCM_{post} techniques as a weighted sum of the M tissue doses, as described in

$$\widetilde{D}_{\text{eff}} = \left(\frac{\sigma}{\sigma_{SmartmA}}\right)^2 \sum_{i=1}^{M} w_i d_i. \tag{1}$$

Medical Physics, Vol. 42 (2015): pg. 6572-6578. DOI.

σ represents the noise standard deviation in the heart and central brain ROIs for chest and head scans, respectively. Scaling by the squared ratio of noise standard deviation adjusts the dose to represent noise equivalent to SmartmA, assuming standard filtered backprojection reconstruction. The tissue weights, w_i, were obtained from ICRP Report 103.[19] The voxelized phantoms used in this study did not have all of the ICRP organs segmented; therefore, the calculated metric represents the approximate effective dose. Organs not segmented in the phantom were assigned a weight of zero. The spinal cord was assigned a weight of 0.01, based on the ICRP weighting for brain tissue. The voxelized phantoms in this study modeled homogeneous cortical bone. The dose to red bone marrow (RBM) was approximated by scaling the cortical bone dose by the RBM mass fraction and the ratio of RBM to cortical bone mass energy attenuation coefficient at the mean energy of the spectrum, similar to the previous studies.[20] The RBM mass fraction was approximated for chest and head scans using the data in the work of Cristy and Eckerman.[21] The dose to segmented regions of soft tissue and muscle was averaged and assigned the remainder tissue weight of 0.12.

3. Results

In the experimental study, ODM reduced the dose at all dosimeter locations compared to SmartmA shown in Fig. 2. When averaged across dosimeters in each tissue region, the dose reductions were 31% (breast), 21% (lung), 24% (heart), 6% (spine), 19% (eye lens), and 11% (brain). Figure 2 also plots the percent change in dose with respect to SmartmA as estimated by the simulation validation study. The experimental and simulation results demonstrated similar trends in dose reduction across the dosimeter locations, as seen in Fig. 2.

Medical Physics, Vol. 42 (2015): pg. 6572-6578. DOI.

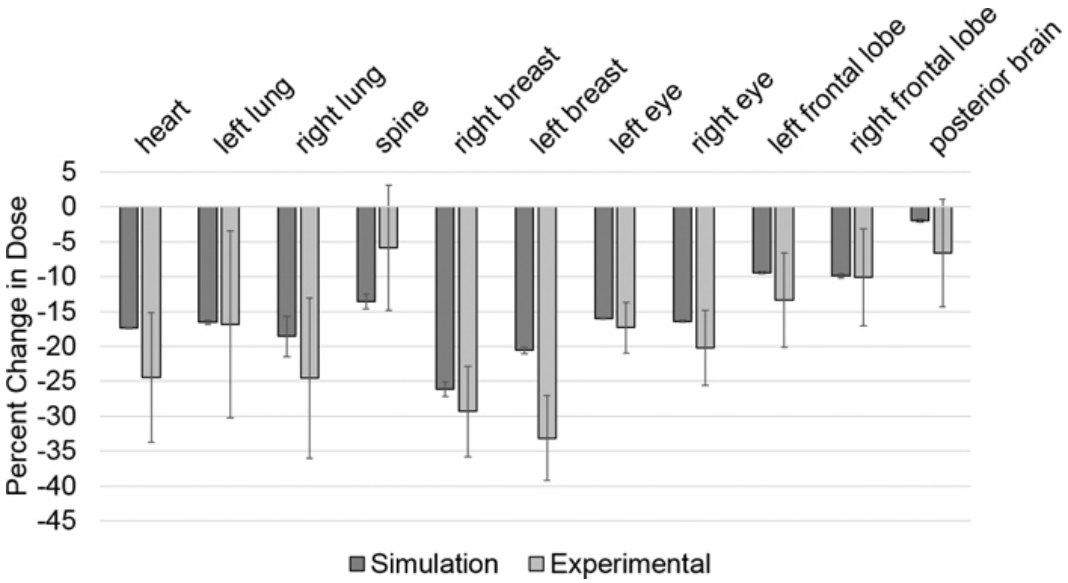

FIG. 2. Comparison of experimental and simulation dose results of ODM with respect to SmartmA for head and chest scans. The error bars represent the standard deviation across the five trials.

Noise standard deviation increased by 8.0% and 4.1% with respect to SmartmA in the experimental head and chest images, respectively. A similar trend was observed in simulated images with an increase in noise by 6.5% in the head and 6.1% in the chest regions with respect to SmartmA.

Table I presents the change in organ dose for ODM and TCM_{post} relative to SmartmA, averaged across all simulated phantoms. ODM reduced dose to all investigated organs relative to SmartmA, with the greatest reduction for the breast and eye lens. TCM_{post} reduced breast and eye lens dose relative to SmartmA, with less dose reduction than ODM. TCM_{post} increased spine dose and provided dose similar to SmartmA for the lung and brain regions.

TABLE I.

Modulation technique	Breast	Lung	Spine	Eye lens	Brain
ODM (%)	−34 ± 1	−20 ± 2	−8 ± 5	−20 ± 2	−7 ± 1
TCM_{post} (%)	−29 ± 2	−1 ± 2	26 ± 3	−16 ± 2	2 ± 1

Percent change in dose for ODM and TCM_{post} relative to SmartmA (mean and standard deviation across the simulated phantoms). A negative percentage represents a decrease in dose.

Medical Physics, Vol. 42 (2015): pg. 6572-6578. DOI.

Only the spine region demonstrated statistically significant correlation between effective diameter and the ratio of ODM dose to SmartmA dose ($p < 0.05$), with a correlation coefficient of 0.7, suggesting that ODM provides less spine dose reduction for larger patients. When the posterior tube current was increased (TCM_{post}), the increase in spine dose relative to SmartmA increased with effective diameter (correlation coefficient of 0.78, $p < 0.01$).

Table II presents the change in noise standard deviation for ODM and TCM_{post} relative to SmartmA, averaged across all simulated phantoms. Both ODM and TCM_{post} demonstrated increased noise compared to SmartmA for anterior and central ROIs, with greater noise increases for ODM than TCM_{post}. TCM_{post} and SmartmA demonstrated similar noise in posterior image regions, while ODM increased noise in posterior regions. The noise increase due to ODM was lower in the posterior regions of the image than the anterior and central regions.

TABLE II.

Modulation technique	Scan type	Anterior (%)	Center (%)	Posterior (%)
ODM	Chest	18 ± 4	20 ± 3	9 ± 4
TCM_{post}	Chest	15 ± 5	17 ± 4	−2 ± 3
ODM	Head	11 ± 3	8 ± 3	6 ± 4
TCM_{post}	Head	8 ± 2	5 ± 3	1 ± 3

Percent change in noise standard deviation for ODM and TCM_{post} relative to SmartmA for three ROI locations (mean and standard deviation across the simulated phantoms). A negative percentage represents a decrease in noise. For chest simulations, the "center" corresponds to a ROI in the heart, while anterior and posterior ROIs were located in the lung. For the head scans, all ROIs were located in the brain.

Figure 3(a) plots the ratio of ODM noise to SmartmA noise versus the ratio of ODM dose to SmartmA dose for all phantoms, while Fig. 3(b) presents the same plot for TCM_{post}. The vertical lines depict the range of noise effects across the three ROIs extracted for each dataset, with the markers located at the median noise ratio. The solid curve is the relationship that noise standard deviation varies inversely proportional to the square root of dose, which is true for filtered backprojection reconstruction if all scan parameters are held constant except for tube current. This relationship may be different for other reconstruction approaches, such as clinically available iterative methods.[22] This boundary line represents no net benefit for ODM or TCM_{post} compared to SmartmA. The shaded area below the line

Medical Physics, Vol. 42 (2015): pg. 6572-6578. DOI.

represents a net reduction in dose at noise standard deviation equal to SmartmA, or conversely a net reduction in noise for ODM or TCM_{post} at an organ dose equal to that of SmartmA. The region above the line represents a net detriment in dose and/or noise. For ODM, the data are plotted at horizontal axis values less than one, demonstrating that ODM reduced the dose to all organs and all phantoms. The vertical values of the ODM data points are greater than one, demonstrating an increase in noise. When comparing the plots for ODM and TCM_{post}, a shift of data points toward higher dose ratios is seen for TCM_{post}. The marker positions in the TCM_{post} plot also demonstrate a median noise increase for TCM_{post} relative to SmartmA. Unlike ODM, TCM_{post} demonstrated reduced noise in the posterior ROIs for some phantoms. The plots demonstrate that both ODM and TCM_{post} resulted in a net dose/noise benefit for breast and eye lens relative to SmartmA, with a net dose/noise detriment for the remaining tissues. The dose/net detriment for the lung, spine, and brain was greater for TCM_{post} compared to ODM.

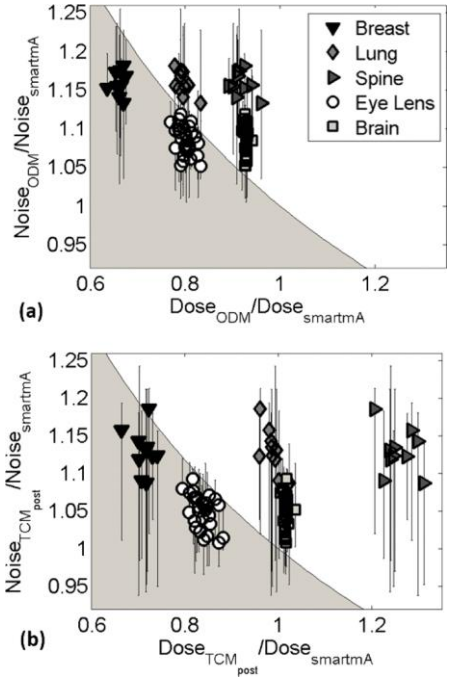

FIG. 3. Relative noise versus relative dose of (a) ODM with respect to SmartmA and (b) TCM_{post} with respect to SmartmA, with each marker representing a different phantom. The vertical bars display the minimum to maximum noise ratios across the regions where noise was measured, with markers located at the median noise levels. The solid curve represents the relationship that noise varies inversely proportional to the square root of dose. The shaded region represents a net dose/noise benefit for the tube current modulation technique relative to SmartmA.

Medical Physics, Vol. 42 (2015): pg. 6572-6578. DOI.

Table III displays the percent change in estimated effective dose, $\widetilde{D}_{\text{eff}}$, for ODM and TCM_{post} relative to SmartmA at equal noise standard deviation. For chest scans, the effective dose of ODM was similar to SmartmA, with half of the phantoms demonstrating effective dose less than or equal to SmartmA and a 4.5% dose increase on average across the simulated phantoms. For head scans, ODM had higher effective dose than SmartmA for all phantoms. TCM_{post} had higher effective dose than ODM for all simulated phantoms and scan types.

TABLE III.

Modulation technique (%)	Scan type	Percent change in $\widetilde{D}_{\text{eff}}$
ODM	Chest	4 ± 7
TCM_{post}	Chest	15 ± 9
ODM	Head	8 ± 6
TCM_{post}	Head	18 ± 6

Percent change in estimated effective dose for ODM and TCM_{post} relative to SmartmA (mean and standard deviation across simulated phantoms). The effective doses are compared at equal noise standard deviation.

4. Discussion

Both simulations and experiments demonstrated that ODM reduced dose to all tissues, but also increased noise, indicating higher noise standard deviation than the prescribed noise index. The noise increase was higher in the anterior regions of the image than the posterior regions of the image, which was expected due to the reduced anterior tube current. In the simulation study, increasing the posterior tube current to maintain the mAs of SmartmA did not recover the noise in the central and anterior image regions, although the noise levels were lower than ODM (Table II). In conventional filtered backprojection reconstruction, the reconstructed image noise is dominated by the noisiest views.[23] The results suggest that the increased tube current in the posterior views, as simulated in this study, did not fully compensate for the reduced anterior tube current for all rays, leading to an overall noise increase compared to SmartmA. The noise performance of ODM and TCM_{post} could potentially be improved by modifying the filtered backprojection algorithm to apply less weight to the noisy anterior views. Iterative reconstruction

Medical Physics, Vol. 42 (2015): pg. 6572-6578. DOI.

could also potentially be used to reduce noise effects due to decreased flux in the anterior views.

The presented effective dose results are approximate, due to the limitations of the simulation study, as described in Sec. 2.C. The results suggest similar effective dose for ODM and SmartmA chest scans, increased effective dose for ODM head scans, and higher effective dose when the posterior tube current is increased. Since the effective dose of ODM and TCM_{post} was compared at noise equal to SmartmA, the effective doses of both methods are expected to decrease if the reconstruction approach is modified to reduce the impact of noisy views. The overall cost versus benefit of reducing dose to the breast/eye lens while increasing noise or dose to the spine/lung/brain requires further study. For example, the eye lens is not included in the calculation of effective dose, but reducing the dose to eye lens may be advantageous in certain cases.

The head and chest experiments were performed at higher dose levels than typical clinical protocols to improve the precision of the dosimeters. The relative changes in dose and noise were calculated between ODM and SmartmA. These relative metrics are theoretically independent of the absolute dose, assuming negligible electronic noise contribution. A supplemental set of experiments imaged the head and chest phantom at SmartmA settings with $CTDI_{vol}$ varying from 5 to 33 mGy, while measuring noise standard deviation with and without the low-signal (electronic noise) correction. The effects of electronic noise and the subsequent low-signal correction did not measurably affect noise standard deviation, suggesting that the relative noise metrics calculated in the experimental ODM study would be valid for typical clinical protocols. The phantom library results demonstrated greater noise increases than the experimental phantom for chest scans, but not for the head scans. This may be due to the modeling of iodine in the phantom library but not the dosimetry phantom.

Several previous studies quantified the dose and image quality of a different commercial ODM implementation (X-Care, Siemens Healthcare, Forchheim, Germany) that reduces tube current by 75% for the 120° arc of anterior views and increases tube current by 25% for the remaining views.[2,4–6] For example, one experimental study using a dosimetry phantom measured breast dose reduction of 35%,

Medical Physics, Vol. 42 (2015): pg. 6572-6578. DOI.

lung dose increase of 2%, no signal-to-noise ratio (SNR) changes in posterior image regions, and SNR decrease of 15% for other image regions.[24] The effective dose was found to decrease by 10% to 15% using this ODM implementation, although at SNR reduced by 15%.[24] A different experimental phantom study demonstrated breast dose reduction ranging from 9% to 45%, lung dose reduction of 2% to 18%, and dose changes in posterior regions ranging from 3% dose reduction to 52% dose increase at noise standard deviation equal to the reference scan.[4] The study estimated a 19% increase in effective dose for the organ-based tube current technique compared to the reference chest scan at equivalent noise.[4] For comparison, the results of the dosimetry phantom in the current study estimate breast dose reduction ranging from 23% to 32%, lung dose reduction of 10% to 20%, and spine dose increase of 2% to 11% when adjusted to represent noise standard deviation equal to that of SmartmA. Direct comparison of the two ODM techniques through simulations is challenging because the alternative commercial implementation modifies the tube current in the anterior and posterior views relative to a different underlying 3D TCM technique.[25]

The angular range of tube current reduction is narrower for the head ODM protocol than the chest ODM protocol. A previous study using a different voxelized phantom suggests that 23% of the eye lens dose is deposited at angles of 50◦ to 80◦ away from the AP view.[26] Therefore, greater eye lens dose reduction may be possible by increasing the angular range of ODM dose reduction for head scans. The ODM settings investigated in this paper were designed for breast and eye dose reduction. Future work should also investigate the performance of ODM for other sensitive anterior organs such as the gonads and thyroid.

5. Conclusions

ODM reduced dose in all experimental and simulation studies over a range of phantoms. However, ODM also increased noise standard deviation. Increasing the posterior tube current to match the total mAs of the reference scan did not fully recover the noise statistics and did not improve the overall dose/noise benefit. When considering both the decreased dose and increased noise, and assuming standard

Medical Physics, Vol. 42 (2015): pg. 6572-6578. DOI.

filtered backprojection reconstruction, the results suggest a net ODM dose benefit for breast and eye lens for all studied phantoms, negligible lung dose effects for two phantoms, increased lung dose and/or noise for eight phantoms, and increased spine dose and/or noise for brain and spine for all studied phantoms.

Acknowledgments

This work was funded in part by GE Healthcare. High performance computing resources were funded by NSF Award No. OCI-0923037. The authors acknowledge the help of Paul Segars (Duke University) for segmenting the glandular breast tissue in the XCAT phantom library models.

References

[1]S. V. Vollmar and W. A. Kalender, "Reduction of dose to the female breast in thoracic CT: A comparison of standard-protocol, bismuth-shielded, partial and tube-current-modulated CT examinations," *Eur. Radiol*. **18**(8), 1674–1682 (2008).http://dx.doi.org/10.1007/s00330-008-0934-9

[2]J. Wang, X. Duan, J. A. Christner, S. Leng, L. Yu, and C. H. McCollough, "Radiation dose reduction to the breast in thoracic CT: Comparison of bismuth shielding, organ-based tube current modulation, and use of a globally decreased tube current," *Med. Phys*. **38**(11), 6084–6092 (2011).http://dx.doi.org/10.1118/1.3651489

[3]X. Duan, J. Wang, J. A. Christner, S. Leng, K. L. Grant, and C. H. McCollough, "Dose reduction to anterior surfaces with organ-based tube-current modulation: Evaluation of performance in a phantom study," *Am. J. Roentgenol*. **197**(3), 689–695 (2011).http://dx.doi.org/10.2214/AJR.10.6061

[4]M. P. Lungren, T. T. Yoshizumi, S. M. Brady, G. Toncheva, C. Anderson-Evans, C. Lowry, X. R. Zhou, D. Frush, and L. M. Hurwitz, "Radiation dose estimations to the thorax using organ-based dose modulation," *Am. J. Roentgenol*. **199**(1), W65–W73 (2012).http://dx.doi.org/10.2214/AJR.11.7798

[5]J. Wang, X. Duan, J. A. Christner, S. Leng, K. L. Grant, and C. H. McCollough, "Bismuth shielding, organ-based tube current modulation, and global reduction of tube current for dose reduction to the eye at head CT," *Radiology* **262**(1), 191–198 (2012).http://dx.doi.org/10.1148/radiol.11110470

[6]Y. K. Kim, Y. M. Sung, J. H. Choi, E. Y. Kim, and H. S. Kim, "Reduced radiation exposure of the female breast during low-dose chest CT using organ-based tube current modulation and a bismuth shield: Comparison of image quality and radiation dose," *Am. J. Roentgenol.* **200**(3), 537–544 (2013).http://dx.doi.org/10.2214/AJR.12.9237

[7]F. Rupcich, A. Badal, L. M. Popescu, I. Kyprianou, and T. G. Schmidt, "Reducing radiation dose to the female breast during CT coronary angiography: A simulation study comparing breast shielding, angular tube current modulation, reduced kV, and partial angle protocols using an unknown-location signal-detectability metric," *Med. Phys.* **40**(8), 081921 (14pp.) (2013).http://dx.doi.org/10.1118/1.4816302

[8]K. D. Hopper, S. H. King, M. E. Lobell, T. R. TenHave, and J. S. Weaver, "The breast: In-plane x-ray protection during diagnostic thoracic CT–shielding with bismuth radioprotective garments," *Radiology* **205**(3), 853–858 (1997).http://dx.doi.org/10.1148/radiology.205.3.9393547

[9]AAPM Board of Directors, "AAPM position statement on the use of bismuth shielding for the purpose of dose reduction in CT scanning. Policy PP-26-A," http://www.aapm.org/publicgeneral/BismuthShielding.pdf, 2012. Accessed August 4, 2014.

[10]D. Zhang, A. S. Savandi, J. J. Demarco, C. H. Cagnon, E. Angel, A. C. Turner, D. D. Cody, D. M. Stevens, A. N. Primak, C. H. McCollough, and M. F. McNitt-Gray, "Variability of surface and center position radiation dose in MDCT: Monte Carlo simulations using CTDI and anthropomorphic phantoms," *Med. Phys.* **36**(3), 1025–1038 (2009).http://dx.doi.org/10.1118/1.3078053

[11]D. Zhang, M. Zankl, J. J. DeMarco, C. H. Cagnon, E. Angel, A. C. Turner, and M. F. McNitt-Gray, "Reducing radiation dose to selected organs by selecting the tube start angle in MDCT helical scans: A Monte Carlo based study," *Med. Phys.* **36**(12), 5654–5664 (2009).http://dx.doi.org/10.1118/1.3259773

[12]J. F. Winslow, C. J. Tien, and D. E. Hintenlang, "Organ dose and inherent uncertainty in helical CT dosimetry due to quasiperiodic dose distributions," *Med. Phys.* **38**(6), 3177–3185 (2011).http://dx.doi.org/10.1118/1.3590367

[13]S. Agostinelli, J. Allison, K. Amako, J. Apostolakis, H. Araujo, P. Arce, M. Asai, D. Axen, S. Banerjee, G. Barrand, F. Behner, L. Bellagamba, J. Boudreau, L. Broglia, A. Brunengo, H. Burkhardt, S. Chauvie, J. Chuma, R. Chytracek, F. Cooperman, G. Cosmo, P. Degtyarenko, A. Dell'Acqua, G. Depaola, D. Dietrich, R. Enami, A. Feliciello, C. Ferguson, H. Fesefeldt, G. Folger, F. Foppiano, A. Forti, S. Garelli, S. Giani, R. Giannitrapani, D. Gibin, J. J. G. Cadenas, I. Gonzalez, G. G. Abril, G. Greeniaus, W. Greiner, V. Grichine, A. Grossheim, P. Gumplinger, R. Hamatsu, K. Hashimoto, H. Hasui, A. Heikkinen, A.

Howard, V. Ivanchenko, A. Johnson, F. W. Jones, J. Kallenbach, N. Kanaya, M. Kawabata, Y. Kawabata, M. Kawaguti, S. Kelner, P. Kent, A. Kimura, T. Kodama, R. Kokoulin, M. Kossov, H. Kurashige, E. Lamanna, T. Lampen, V. Lara, V. Lefebure, F. Lei, M. Liendl, W. Lockman, F. Longo, S. Magni, M. Maire, E. Medernach, K. Minamimoto, P. Mora de Freitas, Y. Morita, K. Murakami, M. Nagamatu, R. Nartallo, P. Nieminen, T. Nishimura, K. Ohtsubo, M. Okamura, S. O'Neale, Y. Oohata, K. Paech, J. Perl, A. Pfeiffer, M. G. Pia, F. Ranjard, A. Rybin, S. Sadilov, E. Di Salvo, G. Santin, T. Sasaki, N. Savvas, Y. Sawada, S. Scherer, S. Sei, V. Sirotenko, D. Smith, N. Starkov, H. Stoecker, J. Sulkimo, M. Takahata, S. Tanaka, E. Tcherniaev, E. S. Tehrani, M. Tropeano, P. Trsucott, H. Uno, L. Urban, P. Urban, M. Verderi, A. Walkden, W. Wander, H. Weber, J. P. Wellisch, T. Wenaus, D. C. Williams, D. Wright, T. Yamada, H. Yoshida, and D. Zschiesche, "G4—A simulation toolkit," *Nucl. Instrum. Methods Phys. Res., Sect. A: Accel., Spectrom., Detect. Assoc. Equip.* **506**(3), 250–303 (2003).http://dx.doi.org/10.1016/s0168-9002(03)01368-8

[14]K. Cranley, B. Gilmore, G. Fogarty, and L. Desponds, "IPEM Report 78: Catalogue of diagnostic x-ray spectra and other data," *Technical Report No*. 78 (The Institute of Physics and Engineering in Medicine (IPEM), 1997).

[15]S. E. McKenney, A. Nosratieh, D. Gelskey, K. Yang, S.-y. Huang, L. Chen, and J. M. Boone, "Experimental validation of a method characterizing bow tie filters in CT scanners using a real-time dose probe," *Med. Phys*. **38**(3), 1406–1415 (2011).http://dx.doi.org/10.1118/1.3551990

[16]M. Berger, J. Hubbell, S. Seltzer, J. Chang, J. Coursey, R. Sukumar, and D. Zucker, "XCOM: Photon cross sections database," *NIST Stand. Ref. Database* **8**, 87–3597 (1998).

[17]W. P. Segars, J. Bond, J. Frush, S. Hon, C. Eckersley, C. H. Williams, J. Feng, D. J. Tward, J. T. Ratnanather, M. I. Miller, D. Frush, and E. Samei, "Population of anatomically variable 4D XCAT adult phantoms for imaging research and optimization," *Med. Phys.* **40**(4), 043701(11pp.) (2013).http://dx.doi.org/10.1118/1.4794178

[18]J. M. Boone, K. J. Strauss, D. D. Cody, C. H. McCollough, M. McNitt-Gray, and T. L. Toth, *Report of AAPM Task Group* 204 (American Association of Physicists in Medicine, College Park, MD,2011).

[19]International Commission on Radiological Protection (ICRP), "The 2007 Recommendations of the International Commission on Radiological Protection. ICRP Publication 103," *Ann. ICRP* **37**, 1–332 (2007).http://dx.doi.org/10.1016/j.icrp.2007.11.001

[20]A. Tzedakis, J. Damilakis, K. Perisinakis, J. Stratakis, and N. Gourtsoyiannis, "The effect of Z overscanning on patient effective dose from

multidetector helical computed tomography examinations," *Med. Phys*. **32**(6), 1621–1629 (2005).http://dx.doi.org/10.1118/1.1924309

[21]M. Cristy and K. Eckerman, "Specific absorbed fractions of energy at various ages from internal photon sources. VI. Newborn," Report No. ORNL/TM-8381, Vol. 6, 1987.

[22]Z. Deák, J. M. Grimm, M. Treitl, L. L. Geyer, U. Linsenmaier, M. Körner, M. F. Reiser, and S. Wirth, "Filtered back projection, adaptive statistical iterative reconstruction, and a model-based iterative reconstruction in abdominal CT: An experimental clinical study," *Radiology* **266**(1), 197–206 (2013).http://dx.doi.org/10.1148/radiol.12112707

[23]M. Gies, W. A. Kalender, H. Wolf, C. Suess, and M. T. Madsen, "Dose reduction in CT by anatomically adapted tube current modulation. 1. Simulation studies," *Med. Phys*. **26**(11), 2235–2247 (1999).http://dx.doi.org/10.1118/1.598779

[24]D. Ketelsen, M. Buchgeister, M. Fenchel, B. Schmidt, T. G. Flohr, R. Syha, C. Thomas, I. Tsiflikas, C. D. Claussen, and M. Heuschmid, "Automated computed tomography dose-saving algorithm to protect radiosensitive tissues: Estimation of radiation exposure and image quality considerations," *Invest. Radiol.* **47**(2), 148–152 (2012).http://dx.doi.org/10.1097/RLI.0b013e3182311504

[25]M. K. Kalra, M. M. Maher, T. L. Toth, B. Schmidt, B. L. Westerman, H. T. Morgan, and S. Saini, "Techniques and applications of automatic tube current modulation for CT," *Radiology* **233**(3), 649–657 (2004).http://dx.doi.org/10.1148/radiol.2333031150

[26]F. Rupcich, A. Badal, I. Kyprianou, and T. G. Schmidt, "A database for estimating organ dose for coronary angiography and brain perfusion CT scans for arbitrary spectra and angular tube current modulation," *Med. Phys*. **39**(9), 5336–5346 (2012).http://dx.doi.org/10.1118/1.4739243

About the Author:

Electronic mail: taly.gilat-schmidt@marquette.edu